International Journal of Applied Earth Observation and Geoinformation 118 (2023) 103289

Contents lists available at ScienceDirect

International Journal of Applied Earth Observation and Geoinformation

journal homepage: www.elsevier.com/locate/jag

Automatic forest change detection through a bi-annual time series of satellite imagery: Toward production of an integrated land cover map

Alonso L. [a,b,*], Picos J. [a], Armesto J. [a,b]

[a] Forestry Engineering School, University of Vigo, A Xunqueira Campus, 36005 Pontevedra, Spain
[b] CINTECX, GESSMin Group (Safe and Sustainable Management of Mineral Resources), 36310 Vigo, Spain

ARTICLE INFO

Keywords:
Forest
Disturbances
Land cover change
Sentinel-2
Small parcels

ABSTRACT

Land cover mapping is fundamental for national and international agencies to monitor forest resources. However, monitoring forest disturbances by direct comparison of these maps poses several difficulties and challenges. As a result, different methodologies have been explored to detect forest disturbances. However, most of them cannot be fully integrated with land cover map production since they require additional input data, while others are not suitable for monitoring small land parcels. This study presents a methodology that fulfils the need to integrate land cover mapping with land cover change detection. Specifically, this methodology was designed to complement the Sentinel-2-based land cover mapping used in Galicia, northwest Spain, a region characterized by small land parceling. First, two previously obtained land cover maps from 2019 and 2020 were compared to identify all the pixels with potential land cover changes using QGIS. The behavior of spectral indexes in a time series were then analyzed to identify which of the previously identified pixels correspond to forest disturbances. This step was implemented in the software R. Using the Normalized Difference Vegetation Index (NDVI) to detect different land cover changes it was obtained an overall accuracy of 82%, considering the existence of varying phenologies, diverse topographic conditions, and areas with a high level of stand fragmentation. This study could help agencies that have already developed their own land cover maps to easily advance the integration of their maps with land cover change detection, since this technique can be applied with any land cover mapping methodology based on multitemporal analysis of satellite images, without the need for additional input data.

1. Introduction

Up-to-date information about the location and evolution of forest resources is fundamental for sustainable forest management and for monitoring their well-being (FAO, 2020). The development of Earth observation programs that provide open-access satellite imagery has spurred a revolution in terms of forest observation and monitoring capabilities, since these programs provide timely and precise information about the Earth's surface (Wulder et al., 2018; Gyamfi-Ampadu and Gebreslasie, 2021; Nitoslawski et al., 2021). The automated production of land cover maps is a key milestone in this new era of forest observation (Wulder et al., 2018). These maps are valuable for providing up-to-date and accurate information about the composition and distribution of forests. Several regional, national, and international programs have endeavored to generate land cover maps adapted to meet the specific needs of stakeholders (Buchhorn et al., 2020; JCyL, 2022, Malinowski et al. 2020, MLRLC, 2019; Serviglobal, 2022; UKCEH, 2021). An example of this at the international level is the land cover maps produced by different European Union agencies. The European Environment Agency has been producing land cover maps at the European level since 1990 (Corine Land Cover) (EEA, 2021). Other European agencies have launched projects, such as the 2017 S2GLC project, to develop methodologies for creating more frequently updated maps with increased spatial resolution (ESA and SEOM, 2017; Malinowski et al. 2020). Efforts by national and even regional agencies have focused on developing their own land cover maps for their specific needs, i.e., increased legend disaggregation or frequency of updates (Alonso et al., 2021; Inglada et al., 2017; UKCEH, 2021). For example, the UK has been producing annual land cover maps using Sentinel-2 data since 2017 (UKCEH, 2021). Given the wide availability of time series of land cover maps, there has been a shift in focus away from the static study of forest resource location and distribution toward a more dynamic monitoring of forest evolution throughout time and the detection of forest disturbances (Addo-Fordjour and Ankomah, 2017; Gilani et al. 2020; Vieilledent

* Corresponding author.
E-mail address: laura.alonso.martinez@uvigo.es (A. L.).

https://doi.org/10.1016/j.jag.2023.103289
Received 13 December 2022; Received in revised form 16 March 2023; Accepted 31 March 2023
Available online 12 April 2023

Table 1
Sentinel-2 band descriptions. Source, ESA (2015).

Band designation	Band name	Central wavelength (nm)	Bandwidth (nm)	Resolution (m)
Band 1	Coastal aerosol	443	21	60
Band 2	Blue	490	66	10
Band 3	Green	560	36	10
Band 4	Red	665	31	10
Band 5	Red edge	705	15	20
Band 6	Red edge	740	15	20
Band 7	Red edge	783	20	20
Band 8	NIR (near infrared)	842	106	10
Band 8A	Narrow NIR	865	21	20
Band 9	Water Vapor	945	20	60
Band 10	SWIR (Shortwave Infrared) - Cirrus	1375	31	60
Band 11	SWIR	1610	91	20
Band 12	SWIR	2190	175	20

et al., 2018).

However, challenges and even significant errors in disturbance detection and reporting have been observed when forest disturbances are monitored via the direct comparison of land cover maps (Alonso et al., 2022b, Buchhorn et al., 2021, Congalton et al., 2014). The main problem is that, when comparing land cover classifications for consecutive time periods, even if they are produced following the same methodology, pixels assigned to a different land cover in an updated map with respect to an earlier map might not correspond unequivocally to disturbances (Alonso et al., 2022b, UKCEH, 2021, Zhu et al., 2020). The comparisons are affected by class-specific errors that blur the real ground truth situation. Some studies state that maps produced along the time series are valuable for monitoring land cover evolution, supporting policy design, and helping in decision-making, since the errors among annual maps often fluctuate spatially across the maps over time, while real changes persist for any given location (UKCEH, 2021). However, other studies point out that land cover maps should be complemented with additional information to aid in the detection and reporting of land cover changes (Alonso et al., 2022b; Buchhorn et al., 2021; Inglada et al., 2017; Wulder et al., 2018).

Bearing this in mind, specific methodologies have been developed to detect forest disturbances. The most efficient methods rely on the analysis of dense time series of satellite images. Common algorithms used are Breaks For Additive Season and Trend (BFAST) (Verbesselt et al., 2010; Verbesselt et al., 2012; Masiliūnas et al., 2021), LandTrendr (Kennedy et al., 2010), and Continuous Change Detection and Classification (CCDC) (Zhu and Woodcock, 2014). These algorithms rely on the analysis of a historical period and the detection of breakpoints in a certain variable that should remain stable throughout the considered time period. The length of the time period considered, the stability of the variable analyzed, and the resolution of the source data greatly impact the accuracy for detecting changes (Gao et al., 2021).

The Copernicus land cover change product (Copernicus, 2020) is an example of using breakpoint analysis in time-series imagery to detect forest changes. Specifically, this product combines the annually produced land cover maps using Sentinel-2 images with the detection of changes, by applying BFAST family algorithms to MODIS time series. This product relies on MODIS as these data provide the required consistent long-term archive of surface reflectance with high temporal frequency to obtain highly accurate results when performing breakpoint detection. However, the coarse resolution of MODIS (250 m) hinders the detection of forest activities affecting only small areas. This is an important limitation since, in certain European regions, the forestry sector is quite active but forest stands are highly fragmented.

Time series of medium spatial resolution satellite images have been explored to detect breakpoints in areas with fragmented forest stands. A study was done using BFAST over sets of Landsat images (30 m) to detect forest disturbances (Esteban Cava et al., 2022). These methods have obtained promising results, although they still present some drawbacks such as difficulty in detecting very small disturbances and the need to apply a supervised classification after detecting breakpoints to decrease errors of commission (Esteban Cava et al., 2022). Multiple studies have indicated the necessity of a supervised classification in fragmented forest areas and in areas with a high phenological change rate or an

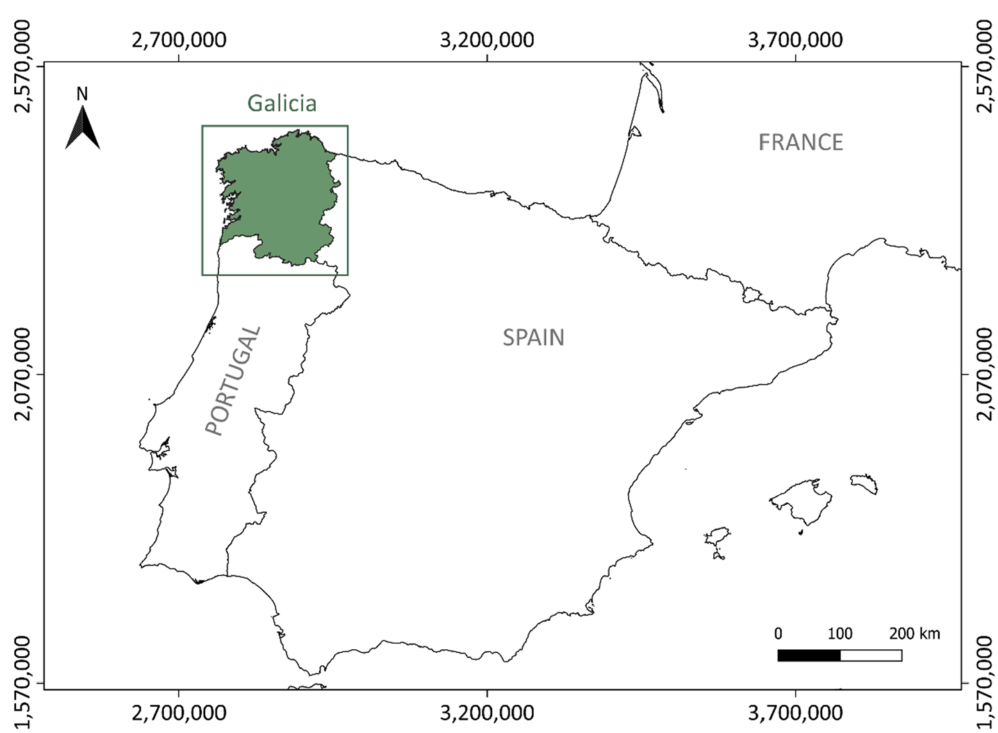

Fig. 1. The study area of Galicia in northwestern Spain.

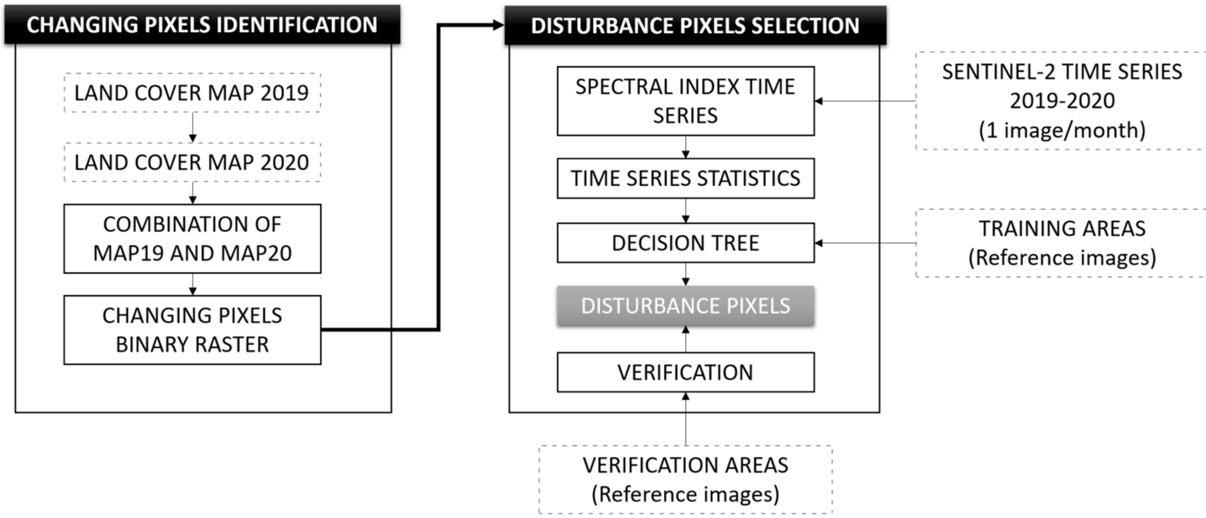

Fig. 2. Methodology overview.

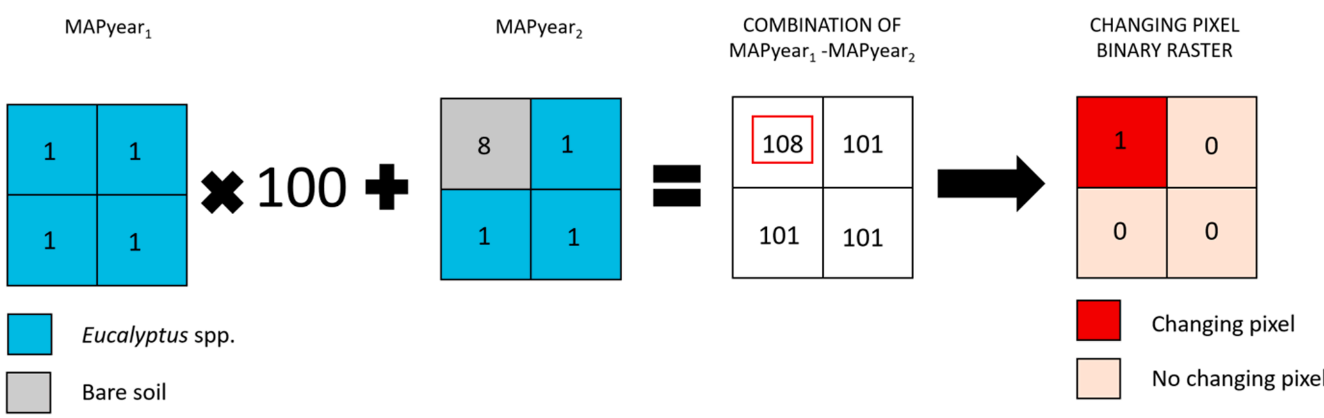

Fig. 3. Workflow to identify changed pixels.

abundance of clouds (Esteban Cava et al., 2022). In fact, studies suggest that, in multiple different environments, supervised classifications are needed to refine the output of the BFAST and LandTrendr algorithms (Xu et al., 2022; Masiliūnas et al., 2021; Shen et al., 2022). Another drawback of the use of these algorithms is the need to analyze very long time series, because this means downloading, organizing, storing, and processing large amounts of data. However, this limitation might be solved by using the cloud computing platform Google Earth Engine, designed specifically to overcome this problem (Gorelick et al., 2017). In fact, multiple studies have already utilized this platform (Chen et al., 2021a; Hamunyela et al., 2020; Mandal and Hosaka, 2020).

A number of studies have explored different methodologies to detect forest changes while avoiding dense time-series analyses (Cardille et al., 2022; Giannetti et al., 2020; López-Amoedo, et al., 2021; Lv et al., 2018). A frequent approach is to explore the behavior of spectral indices in areas previously identified as forest over short time periods, such as 2 (Cardille et al., 2022; Lv et al., 2018) or 3 years (Giannetti et al., 2020). Different techniques have been tested, such as decision trees (Cardille et al., 2022; López-Amoedo, et al., 2021) or change indices (Giannetti et al., 2020). However, given the efforts of multiple different agencies to develop their own self-adapted land cover maps, it would be logical to develop a methodology that integrates existing map production methods with land change detection. Additionally, according to Wulder et al. (2018), the essence of land cover monitoring involves producing an integrated product that provides both land cover and land cover change information.

Therefore, this study proposes a methodology to detect forest disturbances in areas with different topographic conditions, diverse land covers, and varying phenologies. This methodology complements and enhances land cover mapping methodologies that rely on the analysis of time-series satellite imagery. Specifically, this method was designed as part of the land cover mapping protocol that is planned to be used in the new regional forest inventory of Galicia (northwestern Spain) (Xunta de Galicia, 2022a).

2. Material and methods

2.1. Study case

This methodology was developed for Galicia, a region in the northwest of Spain that encompasses a total area of 29.575 km^2. The study area is shown in 1. Galicia has both Atlantic and Mediterranean climates (Meteogalicia, 2022). According to the last forestry report from the government of Galicia in 2016, 48% of the region was covered by forests, which was expected to increase owing to the different policies aimed at promoting forest growth (Xunta de Galicia, 2016). Further, agricultural land abandonment is observed in Galicia, which also contributes to the expansion of forest land (Corbelle-Rico et al., 2022). The main tree species present in Galician forests are *Eucalyptus* spp., *Pinus* spp., *Quercus* spp., and *Castanea* spp., along with species typical of riparian zones such as *Salix* spp. and *Alnus glutinosa* (Xunta de Galicia, 2016). Galicia has an active forest sector (Levers et al., 2014; MITERD,

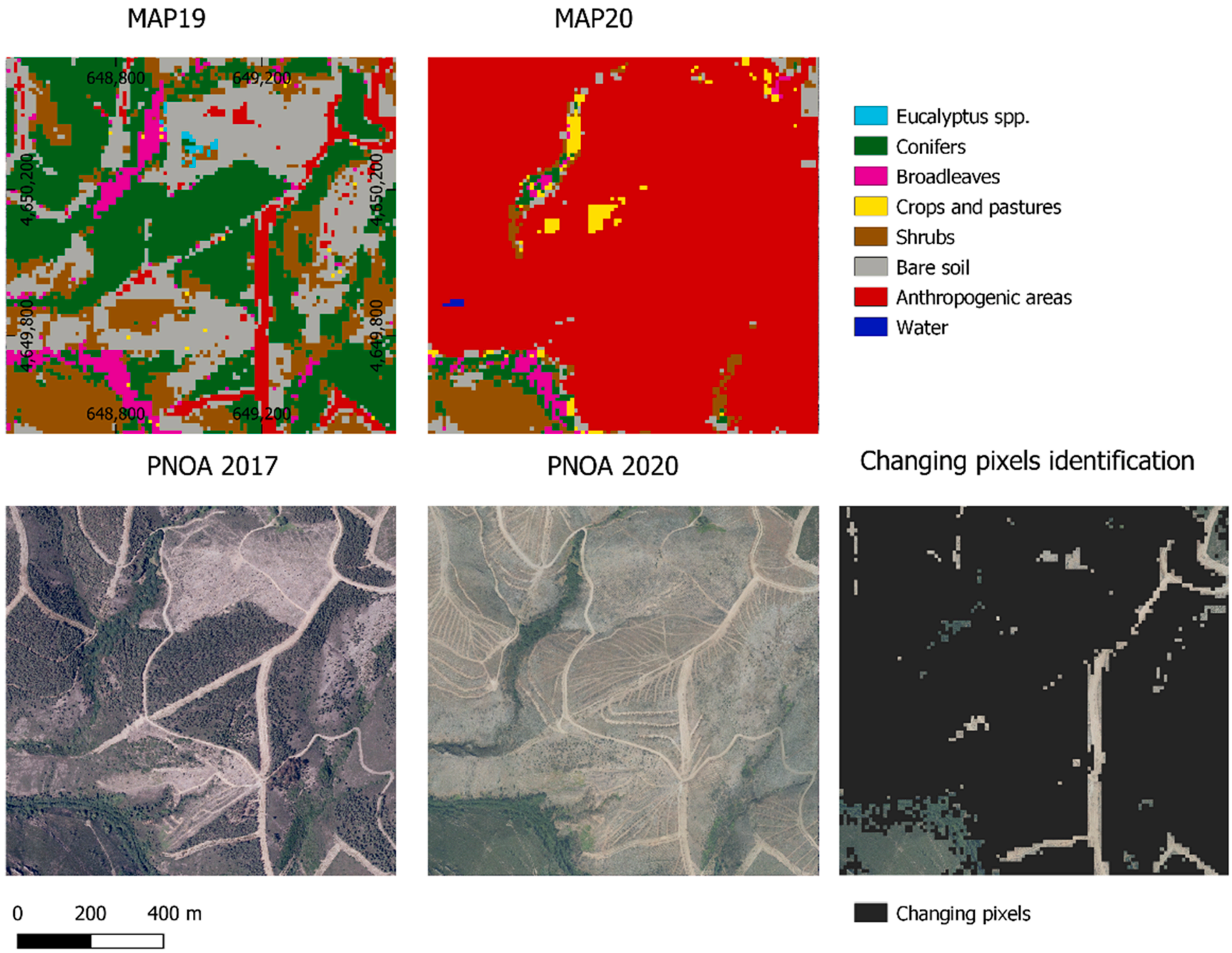

Fig. 4. Example of changed pixel identification in an area that suffered a wildfire.

2018; Xunta de Galicia, 2022b). Additionally, forests in Galicia are highly fragmented: it is estimated that 40% of the productive forest area corresponds to cadastral plots smaller than 0.5 ha (Spanish government, 2011). This results in a large number of small, annually harvested parcels scattered across the whole region. According to the official reports, in the last 7 years (from 2015 to 2021), the regional government has received an average of 83,902 administrative harvesting requests per year, with an average surface area per request of 0.5 ha (Xunta de Galicia, 2022b). As well as harvesting, forests in Galicia are also disturbed by wildfires, being one of the regions in Spain most affected by wildfires (MAPA, 2019; MAPA, 2021).

In view of this, the Galician regional government launched an ambitious research project in 2020, aimed at developing a self-adapted forest inventory that would take into account the idiosyncrasies of the land surface, and could be used to precisely monitor the evolution of forests in Galicia and to design management strategies (Xunta de Galicia, 2022a). Two of the key components of this inventory are (1) to develop methodologies to produce up-to-date forestry-specific land cover maps and (2) to efficiently detect forest disturbances (Xunta de Galicia, 2022a). The first design has already been accomplished and is described in Alonso et al. (2021).

2.2. Materials

2.2.1. Satellite imagery

This methodology relies on Sentinel-2 Level 2A multispectral images (Bottom-of-Atmosphere reflectance). Sentinel-2 is a constellation of two satellites launched by the European Space Agency (ESA) (ESA, 2015). The main aim of the mission is to monitor vegetation systems on the Earth's surface. The mission provides systematic coverage of the entire globe with a high revisit frequency (of between 5 and 10 days). The Sentinel-2 payload instrument captures multispectral information on 13 channels. The spatial resolution of the images obtained ranges from 10 to 60 m, depending on the channel. Information on the bands is outlined in Table 1.

From the Sentinel-2 products available for download (European Commission and ESA, 2022), the Level 2A product (analysis ready data product) was selected. The images were downloaded from the Copernicus Open Access Hub (European Commission and ESA, 2022).

For the years 2019 and 2020, one image per month and per tile was downloaded, for a total of 24 images per Sentinel-2 tile. The criteria used to select the image to represent each month was the same as that used by Alonso et al. (2021). For each month, the image with the minimum cloud percentage was selected, with the condition that the cloud percentage would never surpass 50%. In cases where no images met this threshold, an additional image from the previous or following month was selected (see Fig. 1).

2.2.2. Reference images

Reference data were obtained from aerial orthorectified images (PNOA images) (MTMAU, 2022). The Spanish National Cartographical Institute (IGN) (MTMAU and IGN, 2022) provides open-access images

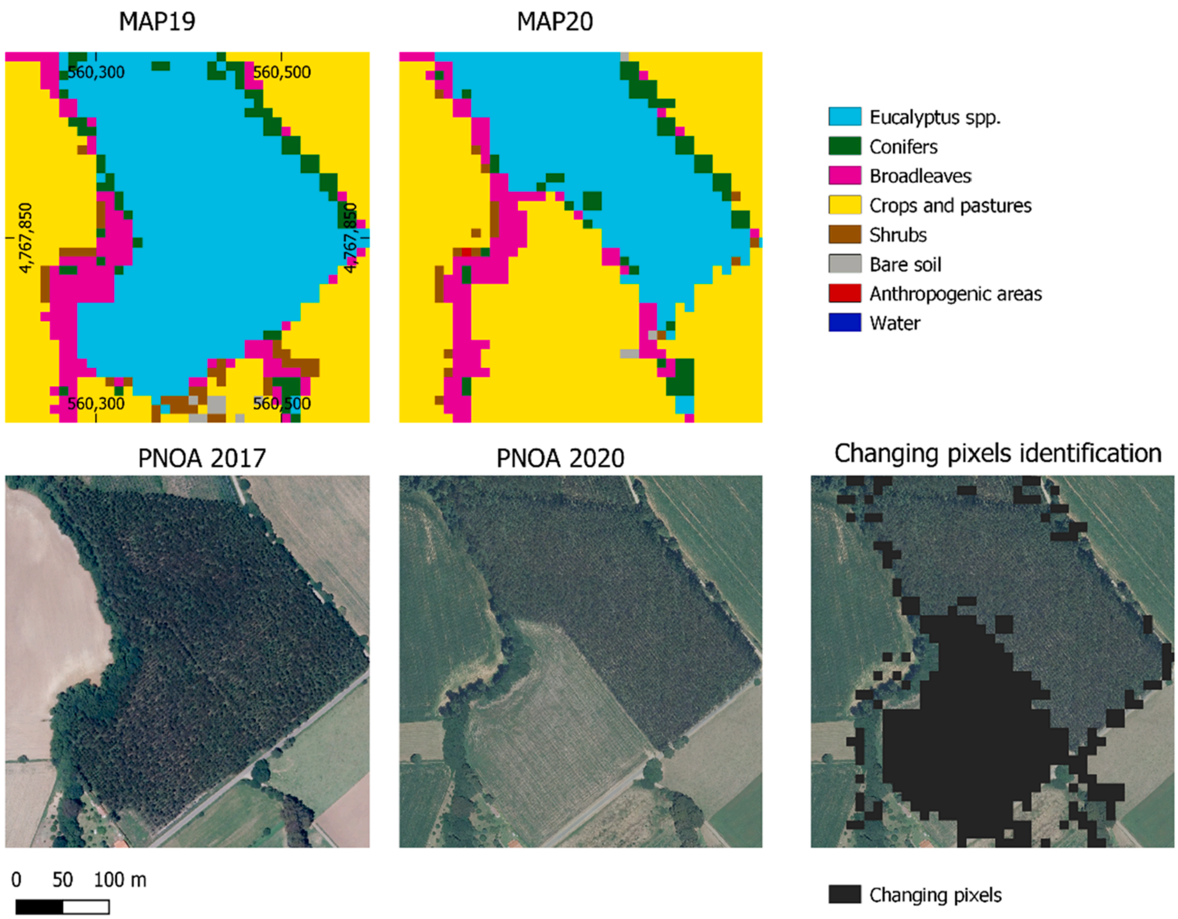

Fig. 5. Example of changed pixel identification in an area that was harvested.

from two photogrammetric flights performed in 2017 and 2020 for Galicia. The spatial resolutions for the 2017 (PNOA 2017) and the 2020 (PNOA 2020) images are 0.25 and 0.15 m, respectively. The georeferencing mean square errors for the 2017 and 2020 images are ≤ 0.50 and ≤ 0.20 m, respectively (MTMAU, 2022).

2.2.3. *Land cover maps*

The starting point for this study was two forestry-oriented land cover maps of Galicia: a 2019 land cover map (MAP19) and a 2020 land cover map (MAP20). The maps were obtained from Alonso et al. (2022b) and created following the same methodology, described in detail in Alonso et al. (2021 and 2022b) and based on supervised classifications of Sentinel-2 images. The legend for the maps is as follows: *Eucalyptus* spp., conifers, broadleaves, shrubs, crops and pastures, bare soil, anthropogenic areas, and water. The overall accuracies of the maps are 86% for MAP19 and 88% for MAP20. Further accuracy metrics can be found in Alonso et al. (2022b).

2.3. *Methodology*

The aim of this method is to identify, from the land cover map comparison, which of the pixels that changed land cover class from the classification in one year to the next actually correspond to forest disturbances. The method has two main steps: (1) identifying changing pixels and (2) selecting disturbance pixels. The first step involves pixel-to-pixel comparisons, while the second step analyzes the behavior of spectral indices along a time series. The time series started in January 2019 and ended in December 2021. Fig. 2 shows an overview of the methodology.

2.3.1. *Identification of changed pixels*

To identify all pixels where the land cover potentially changed from 2019 to 2020, MAP19 and MAP20 were combined to obtain a single raster reflecting the land cover for both years. For this, raster calculations were performed using the raster calculator in QGIS (QGIS.org, 2022). In this particular case, MAP19 was multiplied by 100 and added to MAP20, giving the following coded digital values of pixels: the first digit (hundreds) corresponds to the 2019 land cover class, and the third digit (units) to the 2020 land cover class. Wherever the land use for a pixel in MAP19 and MAP20 matched, the first and third digits of the new raster also matched. However, if the first and third digits are different, then that pixel is identified as a change pixel. A list of mismatch codes was then defined according to the codes of the land cover classes, enabling the identification of changed pixels and the creation of a binary raster containing their distribution.

Once the changed pixels were identified, the downloaded images were masked in such a way that only the spectral information of the changed pixels was retained, while the rest of the pixels were changed to "no data." This process serves to reduce the amount of information to be processed in the following steps. Fig. 3 illustrates this processing step.

2.3.2. *Selection of disturbance pixels*

Disturbance pixels were selected by analyzing the behavior of the spectral indices of pixels identified in the previous step throughout the study period. The indices analyzed were the Normalized Difference Vegetation Index (NDVI) (Kogan 1995; Tarpley et al., 1984) and the Normalized Burn Ratio (NBR) (Key and Benson, 2003). The NDVI is commonly used to assess the greenness of land cover, since it is highly sensitive to chlorophyll content (Kogan 1995; Tarpley et al., 1984). It uses the near infrared (NIR) and red channels of multispectral images

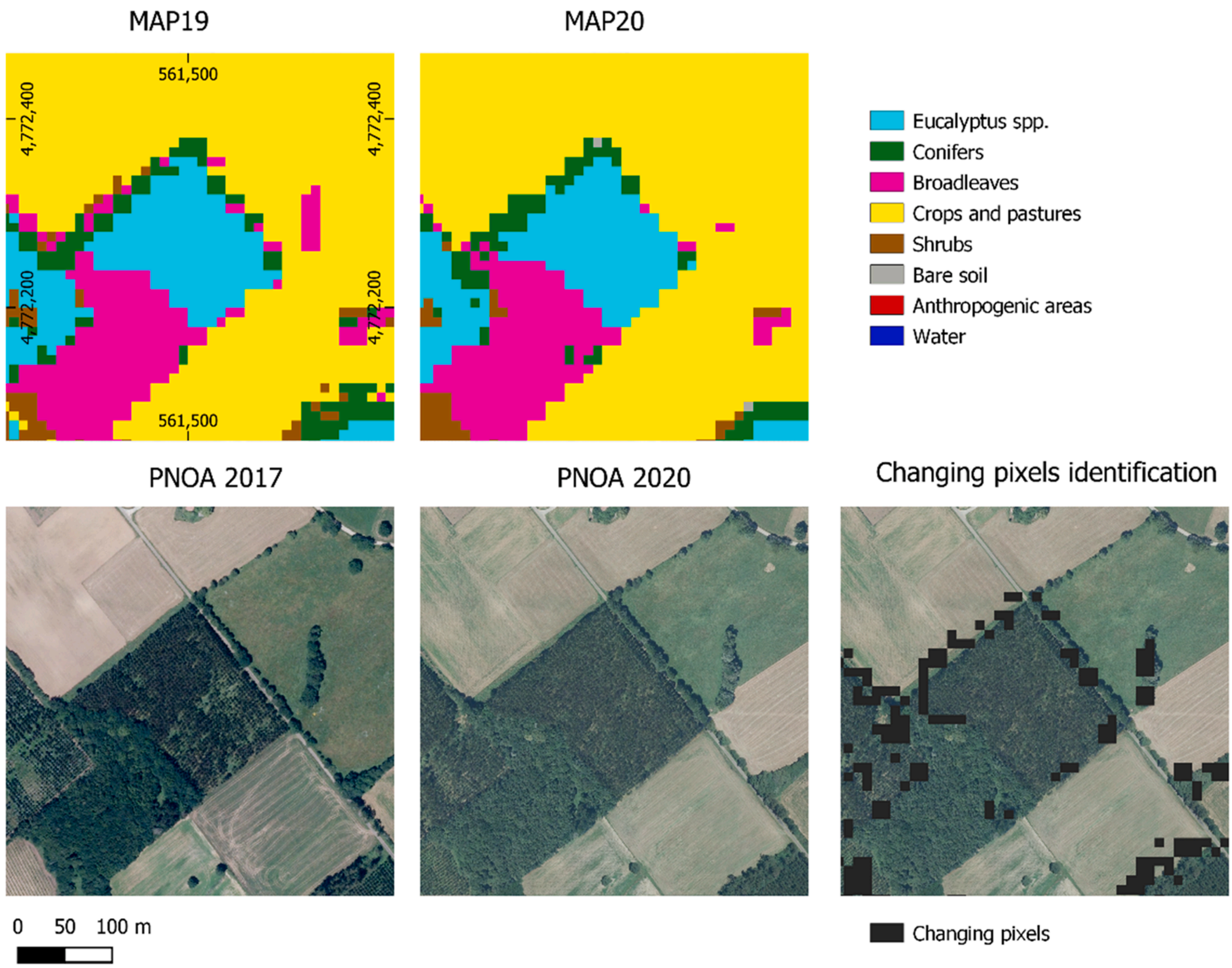

Fig. 6. Example of changed pixel identification due to edge effects.

(Equation 1), which are bands 8 and 4, respectively, in Sentinel 2.

$$NDVI = \frac{NIR - RED}{NIR + RED}$$

Equation 1. NDVI formula. NIR: near infrared, Sentinel-2 band 8; RED: Sentinel-2 band 4.

The NBR is commonly used to identify burned areas through satellite imagery analysis (Key and Benson, 2003). It uses the shortwave infrared (SWIR) and NIR channels of multispectral images (Equation 2), which are bands 12 and 8, respectively, in Sentinel-2.

$$NBR = \frac{NIR - SWIR}{NIR + SWIR}$$

Equation 2. NBR formula. NIR: near infrared, Sentinel-2 band 8; SWIR: shortwave infrared, Sentinel-2 band 12.

Both indices have been used previously to detect forest disturbances (Cardille et al., 2022; Chen et al, 2021b; Gao et al., 2019; Tian et al., 2018; Zhou et al., 2021). Some studies have also focused on identifying which index performs better, although the results thus far have been inconclusive and depend on the context (Zhou et al., 2021; Hislop et al., 2019; Bueno et al., 2020). For this reason, in this study, both indices were explored.

Before calculating the indices, the masked downloaded images were preprocessed to remove any cloud pixels that might greatly interfere with the subsequent analyses. Clouds were removed using the cloud layer that includes the Level 2A product. Upon preprocessing the images, the NDVI and NBR were calculated, giving the spectral behavior of the changing pixels for the months analyzed.

To summarize the behavior of the spectral indices throughout the time series, the following statistics were then calculated for each pixel and for each spectral index: maximum; minimum; average; standard deviation; median; variance; skewness; and the 5th, 10th, 50th, 90th, and 95th percentiles. The next steps use these statistics to identify changing pixels that correspond to a disturbance among all the changing pixels. All these steps were conducted in the R software (R Core Team, 2020).

A set of training data was defined: a random sample of points selected from among the previously identified changing pixels. Each point was inspected in detail to determine whether it corresponded to a change (a disturbance) or if, in fact, no change had occurred (a non-disturbance). A change was defined as any decrease in vegetation due to a disturbance, for example, timber logging or a forest fire. The inspection was performed through photointerpretation of Sentinel-2 and PNOA images from 2017 and 2020. If a disturbance was observed in the 2017 and 2020 PNOA images, that point was further inspected in the Sentinel-2 images to verify that the change had indeed occurred in the time frame of interest (from 2019 to 2020). If this could be confirmed, the pixel was included in the training data as a disturbance point. However, if no disturbance was observed between the 2017 and 2020 images, that point was further analyzed in the Sentinel-2 images to confirm that indeed no disturbance had occurred in 2020, even after the acquisition of the PNOA image. If it was confirmed that no disturbance

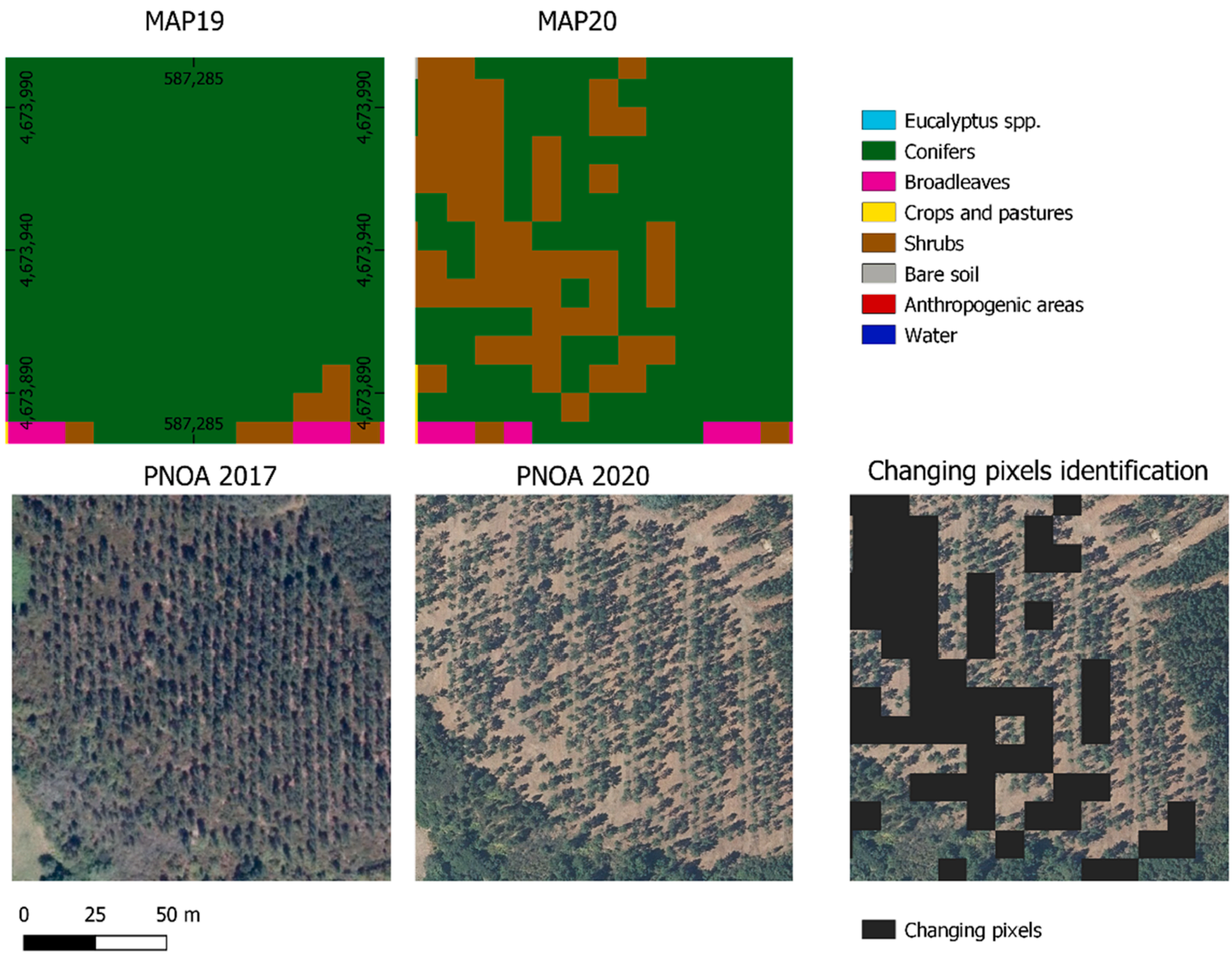

Fig. 7. Example of changed pixel identification in an area that had undergone slashing.

had occurred, the pixel was included in the training data as a non-disturbance point. Care was taken to procure training data representative of the most common disturbances present in the study area (both harvests and wildfires), and the driver of the disturbance was also interpreted in the PNOA and Sentinel-2 images. In cases where it was not possible to determine whether a point was a disturbance or not through photointerpretation, the point was removed from the sample.

Once the indices were calculated and the training sets defined, a decision tree was built using R software to establish the thresholds that would distinguish between pixels that corresponded to disturbances and pixels that corresponded to non-disturbances. A decision tree is an easy-to-use machine learning approach for performing supervised classifications (Breiman et al., 1984) that could potentially be implemented with future datasets. The decision tree was built and applied using the "rpart" library in R software, with default parameters (Therneau and Atkinson, 2019). The resulting decision tree was applied to all of the potential disturbance pixels to identify which of them in fact corresponded to real disturbances.

The obtained results were cross verified. A random stratified sample of 500 points was created: 250 pixels classified as non-disturbances and 250 pixels classified as disturbances. The real land cover of the sample was obtained through interpretation of the reference images (PNOA 2017 and 2020) and Sentinel-2 images, following the same strategy as that used to obtain the training data. A confusion matrix was built and the overall accuracy (OA), users accuracy (UA), and producers accuracy (PA) were calculated. This procedure was performed for both the NDVI and NBR indices. The final accuracy metrics obtained were compared to determine which index was most appropriate for this method.

3. Results

3.1. Changed pixel identification

In total, 14,909,340 changed pixels were identified, corresponding to 20% of the surface area of Galicia. Figs. 4–8 show examples of identified changed pixels. In Figs. 4 and 5, changed pixels are shown in an area where a certain disturbance took place: a wildfire and a timber harvest, respectively. Figs. 6, 7, and 8, on the other hand, correspond to examples of areas where changed pixels were detected but no disturbance has occurred. Fig. 6 is an example of changed pixels being detected due to edge effects. Fig. 7 shows changed pixels that were identified in a stand that had undergone slashing. In 2019, this stand was identified as pine, but the next year some of the pixels in the stand were identified as shrubs by the radiometry of the understory, which exceeded the radiometry of the canopy as a result of the treatment received. The final image (Fig. 8) corresponds to changed pixels identified in a young stand that is growing. In the first year, the stand was wrongly classified as broadleaves, but as the canopy began to fill in, the stand was then correctly classified as eucalyptus.

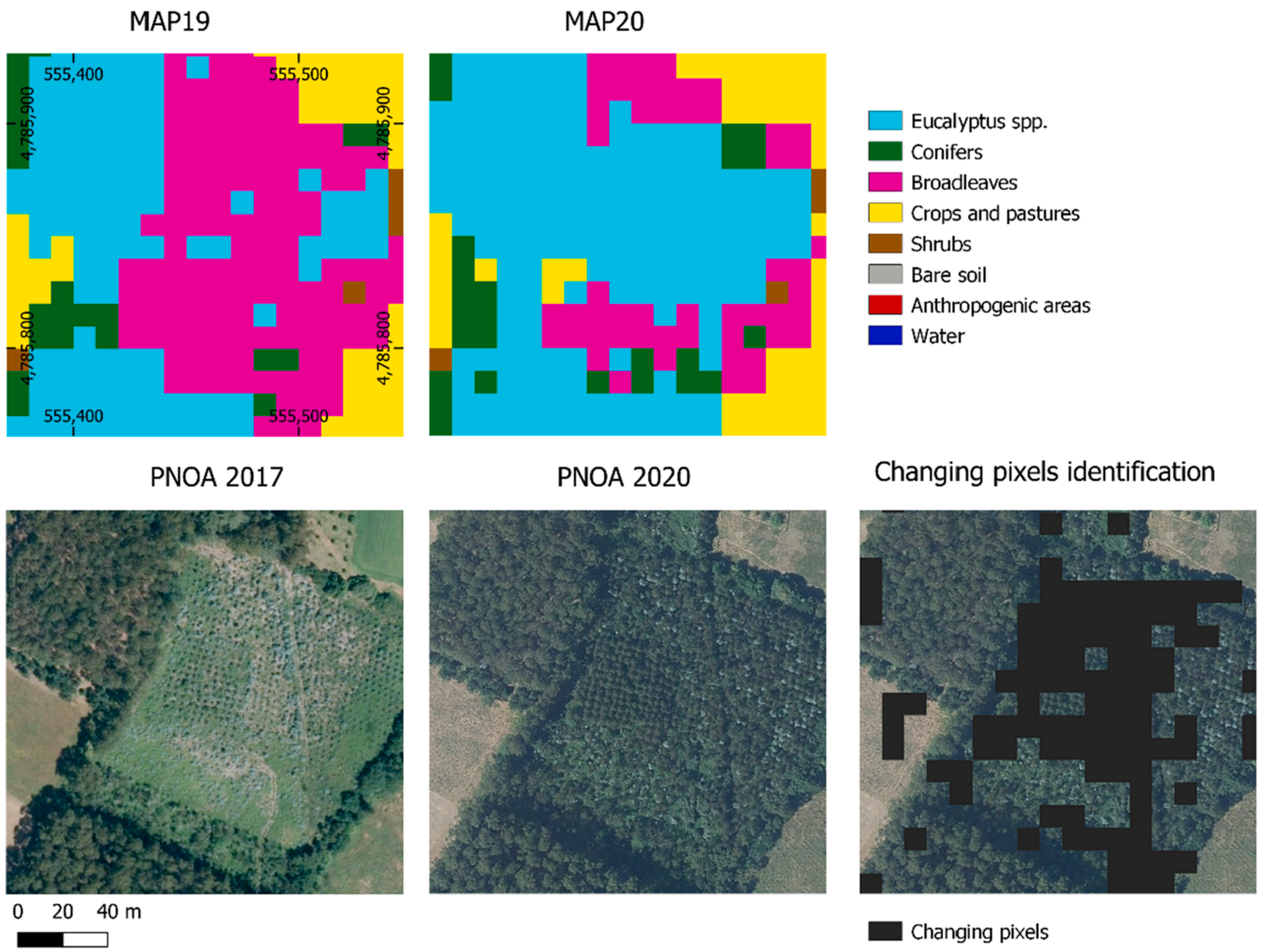

Fig. 8. Example of changed pixel identification in an undisturbed area of a young eucalyptus stand growing.

3.2. Disturbance pixel selection

The evolution of the NDVI values over the studied time series is shown for two points in Fig. 9: one point corresponds to an undisturbed eucalyptus stand, and the other point corresponds to a disturbed (harvested) eucalyptus stand. The behavior lines illustrate the different profiles of both cases. Sentinel-2 images captured at different dates in false color (B8, B4, and B3) are shown to help explain the histogram of the disturbed plot. Additionally, a high-resolution image (PNOA 2017 and PNOA 2020) of the disturbed plot is shown.

A total of 749 points were used to train the decision tree: 478 non-disturbance points and 271 disturbance points. The decision trees obtained for the NDVI and the NBR are shown in Figs. 10 and 11, respectively. Both trees used the 10th percentile as the first criterion to differentiate between disturbances and non-disturbances. The other metrics included in the decision tree for the NDVI were skewness and standard deviation, while the NBR decision tree also selected the 90th percentile. The thresholds for each branch of the two trees were quite similar.

Application of the decision trees led to the identification of 1,930,879 disturbance pixels for the NDVI and 4,734,549 disturbance pixels for the NBR. The results are shown in Fig. 12 where they can be compared with the changed pixels identified in the comparison of the two land-cover maps.

Tables 2 and 3 present the confusion matrices obtained after applying the NDVI and NBR decision trees, respectively, to all the identified changed pixels. Greater overall accuracy was obtained when using the NDVI, which is mostly due to the high number of false-positive disturbances reported by the NBR. The proportion of true positives, with a user's accuracy of 98% in both confusion matrices, highlights the advantage of using both indices for analysis.

The verification results were further analyzed, considering the type of disturbance identified in the reference data. The results are presented in Tables 4–7. A high percentage of the disturbances correspond to harvestings (94% for the NDVI and 95% for the NBR), as expected considering the ratio of harvestings and wildfires in the study area. Tables 4 and 6 present the results in absolute values, and Tables 5 and 7 in relative values. Tables 5 and 7 show that small percentages of each type of disturbance are undetected by the algorithms. Finally, in the NBR, the percentage of detected wildfires is slightly higher than in the NDVI.

Graphical examples of the performance of the decision trees for both indices are shown in 13. Fig. 13a shows a harvesting event that was correctly detected by the NDVI and the NBR. Fig. 13b shows an example of an error of commission when applying the NBR. The reference images show that it is an area where pine is growing and therefore some pixels are most commonly detected as pine throughout the year, while others are sometimes identified as shrubs because the radiometry detected is that of the understory. This method provides a solution to this problem, as it correctly identifies these pixels as undisturbed. Fig. 13c shows an example of an area correctly identified as undisturbed. This area presented an absence of trees in 2017 and is where eucalyptus had been planted and was starting to grow. It is true that a land cover change occurred; however, it is not a disturbance but rather a vegetation

Fig. 9. NDVI values over the studied time series of an undisturbed eucalyptus stand and a disturbed eucalyptus stand. Sentinel-2 images captured at different dates in false color (B8, B4, and B3) are shown to help explain the histogram of the disturbed plot. PNOA 2017 and PNOA 2020 are high-resolution images of the disturbed plot.

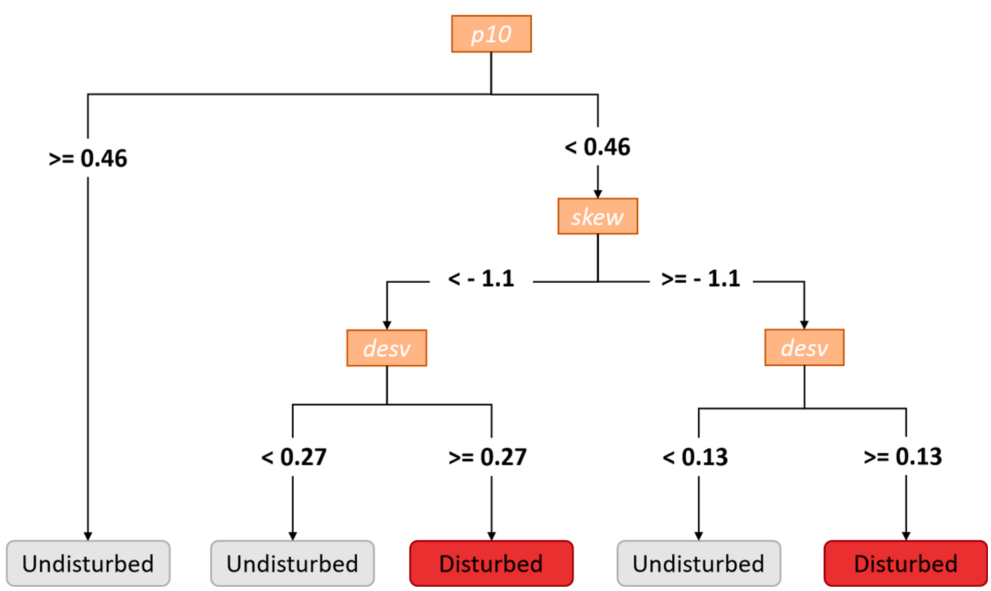

Fig. 10. Decision tree obtained for the NDVI.

recovery, and therefore the algorithm, as expected, identified it as a non-disturbance. Fig. 13d shows an example of a very small harvest area correctly detected by the algorithm. Additionally, in Fig. 13 d), another harvested area appears that was not analyzed because it was not identified as part of the changed pixels. This could be because it might have been a late harvest in 2020 and therefore the 2020 land cover map still identifies it as trees. When using this method, late harvesting events, such as this one, will be identified in the following years analysis (comparison of 2020 and 2021 maps). Fig. 13e shows an area covered by shrubs and trees in 2017 that suffered a wildfire in 2020. This disturbance was correctly identified by both the NDVI and the NBR.

4. Discussion

The methodology outlined herein is capable of detecting changes that occur in different land covers with varying phenologies, as well as in areas with differing topographic conditions. It was also efficient in areas with a great degree of stand fragmentation, as shown in Fig. 12, a

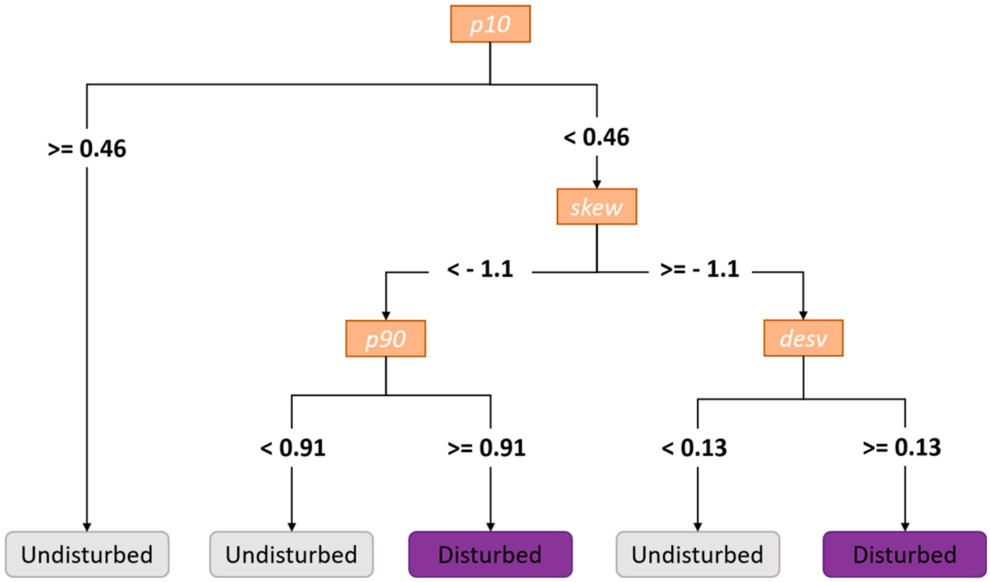

Fig. 11. Decision tree obtained for the NBR.

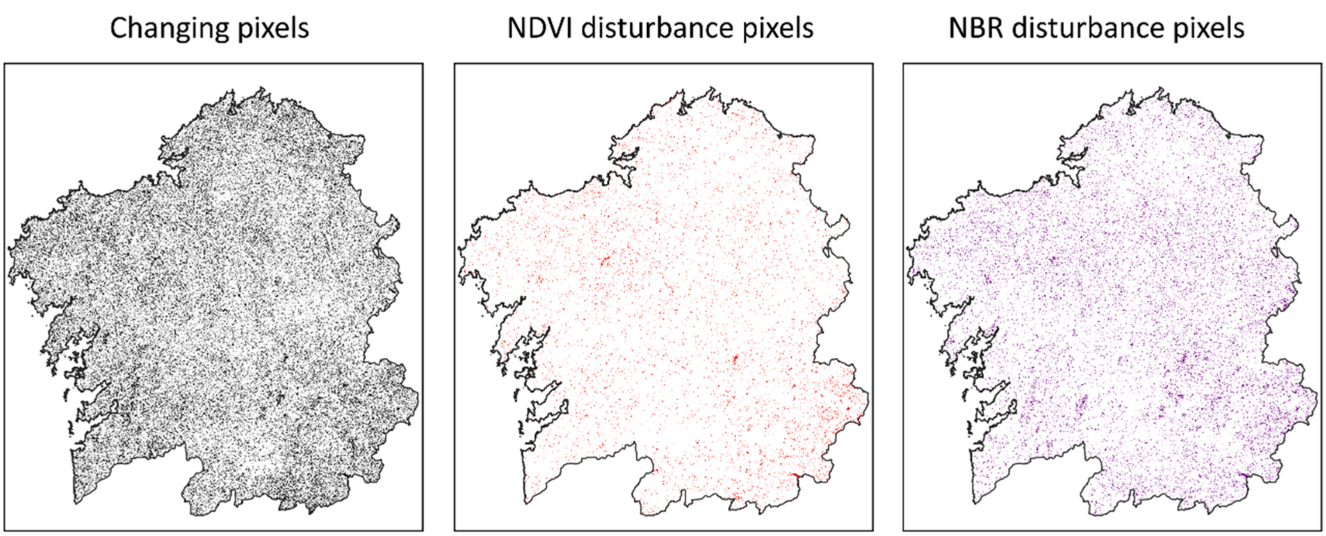

Fig. 12. Comparison between changed pixels identified and the disturbances detected at these pixels using the NDVI and NBR.

Table 2
Results of the NDVI verification: producer's accuracy (PA), user's accuracy (UA), and overall accuracy (OA).

	Decision tree results			
Reference data	Undisturbed	Disturbed	TOTAL	PA
Undisturbed	244	86	330	74%
Disturbed	6	164	170	96%
TOTAL	250	250	500	**OA**
UA	98%	66%	**OA**	82%

Table 3
Results of the NBR verification: producer's accuracy (PA), user's accuracy (UA), and overall accuracy (OA).

	Decision tree results			
Reference data	**Undisturbed**	**Disturbed**	**TOTAL**	**PA**
Undisturbed	247	147	394	63%
Disturbed	3	103	106	97%
TOTAL	250	250	500	**OA**
UA	98%	41%	**OA**	70%

phenomenon that is quite common in the study area. This methodology provides a reliable alternative to methodologies that rely on breakpoint detection in a dense time series of images with coarse spatial resolution, such as those proposed by Esteban Cava et al. (2022) and Buchhorn et al. (2021). However, a detailed comparison of the results of this study and those obtained by Esteban Cava et al. (2022) could be carried out to evaluate the applicability of each method for cases of very small harvesting areas in this study area.

The disturbance detection methodology was designed to be compatible and easily integrated with the land cover mapping methodology designed for Galicia. Both processes can be performed in parallel since they rely on the same sets of monthly Sentinel-2 images (Alonso et al. 2022b): the 12-image sets that are used to create the annual land cover maps can also be used in the image series for disturbance detection. Therefore, this method does not require additional datasets, nor extra downloading, resampling, and processing. This

Table 4
Disturbance class data obtained by the NDVI, considering the type of disturbance detected in the reference data.

	Reference					
	Undisturbed		Disturbed		TOTAL	
	N	Percentage	*N*	Percentage	*N*	Percentage
Wildfire	1	17%	10	6%	11	6%
Harvesting	5	83%	154	94%	159	94%
TOTAL	6	100%	164	100%	170	100%

Table 5
Relative values of disturbance class data obtained by the NDVI, considering the type of disturbance detected in the reference data.

	Reference		
	Undisturbed	Disturbed	
Wildfire	9%	91%	100%
Harvesting	3%	97%	100%

is the main difference between this methodology and those developed by Cardille et al. (2022) and Giannetti et al. (2020). For example, Cardille et al. (2022) use all the available Landsat and Sentinel-2 images in a 2-year period that have a cloud cover of less than 50%. Their methodology, which entails a significant increase in stored information and computational time, also analyzes data at a coarser resolution, given that the pixel size of Landsat images is 30 m (Cardille et al. 2022). This is not desirable for this study region due to its high level of fragmentation.

The highest accuracies were obtained when using the NDVI, with an overall accuracy of 82%. The accuracies were lower when using the NBR owing to the high number of false positives obtained with this spectral index. This result contradicts the results obtained in other studies relying on the NBR, such as the study by Cardille et al. (2022), in which the PA and the UA were both above 75%. Similarly, Zhou et al. (2021) obtained higher accuracies with the NBR than with the NDVI. Therefore, the decision of which index to apply may depend, as suggested by Bueno et al. (2020), on the methodology, the type of disturbance to assess, and the type of vegetation analyzed.

It should be noted that the highest overall accuracy achieved in this study is somewhat lower than the values reported in the scientific literature for analogous methodologies, which generally range from 88% to 99% (Cardille et al., 2022; Giannetti et al., 2020; López-Amoedo et al., 2021). This is because the size of the disturbances tend to be larger in other methodologies. The study by López-Amoedo et al. (2021) is an exception, as it focuses on small harvesting events similar to the disturbances analyzed here. However, their study analyzes only two genera of forest stands, and their methodology is designed to detect disturbances and evaluate accuracy at the parcel level. Consequently, the overall accuracies cannot be compared directly. Furthermore, all these previous methodologies are based on either a preexisting forest mask (Cardille et al., 2022; Giannetti et al., 2020) or a selection of cadastral plots that are known to be forest land (López-Amoedo et al., 2021). Masks are prone to classification errors and can require continual updating in areas with intense land cover dynamics, while declarations (the basis of cadastral parcel analysis) can deviate from reality for multiple reasons (López-Amoedo et al., 2021), so these methods ought to be complemented with intensive photointerpretation work. The methodology presented herein is especially valuable for regions such as Galicia with highly dynamic forests, since it can be applied directly to the whole territory and any type of forest stands, without the need for a forest mask or intensive photointerpretation.

This study reveals that, given the high number of changed pixels with respect to true forest disturbances, forest changes cannot be derived simply from the comparison of land cover maps from consecutive years in areas with intense forest dynamics and where stands are highly fragmented. Refinement procedures, such as that presented herein, are essential. Edge pixels play an important role, as shown in Fig. 6 since, in a small parcel system, a high percentage of the area may correspond to edge pixels. Sentinel-2 miss-registration issues (Kukawska et al., 2017) may augment edge effects (Mi et al., 2022), therefore research on co-registration of Sentinel-2 images may be crucial for these kinds of regions.

Detecting changed pixels is an important starting point in forest disturbance reporting and forest stand monitoring, and the methodology presented in this study does this efficiently. Once the disturbance pixels are confirmed, it might be interesting to analyze the driver generating the disturbance (i.e., harvesting activity or wildfires), as in the study by Cardille et al. (2022). Using the methodology of Alonso et al. (2022a) to distinguish disturbance drivers could be an interesting complement to the methodology described herein since it does not require any additional information as it relies on the analysis of the disturbance geometry. Furthermore, since the confirmed disturbances are georeferenced, they can be analyzed with earlier land cover maps to quantify changes in relation to the type of cover affected, and to evaluate the spatial distribution of the disturbances, if needed. Finally, an in-depth analysis could be performed to investigate how best to deal with changed pixels that do not correspond to disturbances. It is crucial to develop territory-specific workflows, such as those designed by Abercrombie and Friedl (2015) and Zhu et al. (2020), to update land cover maps. An essential part of creating this workflow is an in-depth exploration, similar in nature to the analysis performed by Alonso et al. (2022b), of the correspondence between land cover maps and reality.

Although the method presented herein was specifically designed for Galicia, it is compatible with other land cover mapping methodologies such as those by Inglada et al. (2017) and the UKCEH (2021). For example, this methodology could allow the UKCEH to detect disturbances without the need to acquire additional input data, and thus resolve their current issue of having to wait long periods of time to discern whether pixel changes are permanent in time and hence correspond to disturbance or they are mapping error related (UKCEH, 2021).

Table 7
Relative values of disturbance class data obtained by the NBR, considering the type of disturbance detected in the reference data.

	Reference		
	Undisturbed	Disturbed	
Wildfire	0%	100%	100%
Harvesting	3%	97%	101

Table 6
Disturbance class data obtained by the NBR, considering the type of disturbance detected in the reference data.

		Reference				
	Undisturbed	Disturbed	TOTAL			
	N	Percentage	*N*	Percentage	*N*	Percentage
Wildfire	0	0%	5	5%	5	5%
Harvesting	3	100%	98	95%	101	95%
TOTAL	3	100%	103	100%	106	100%

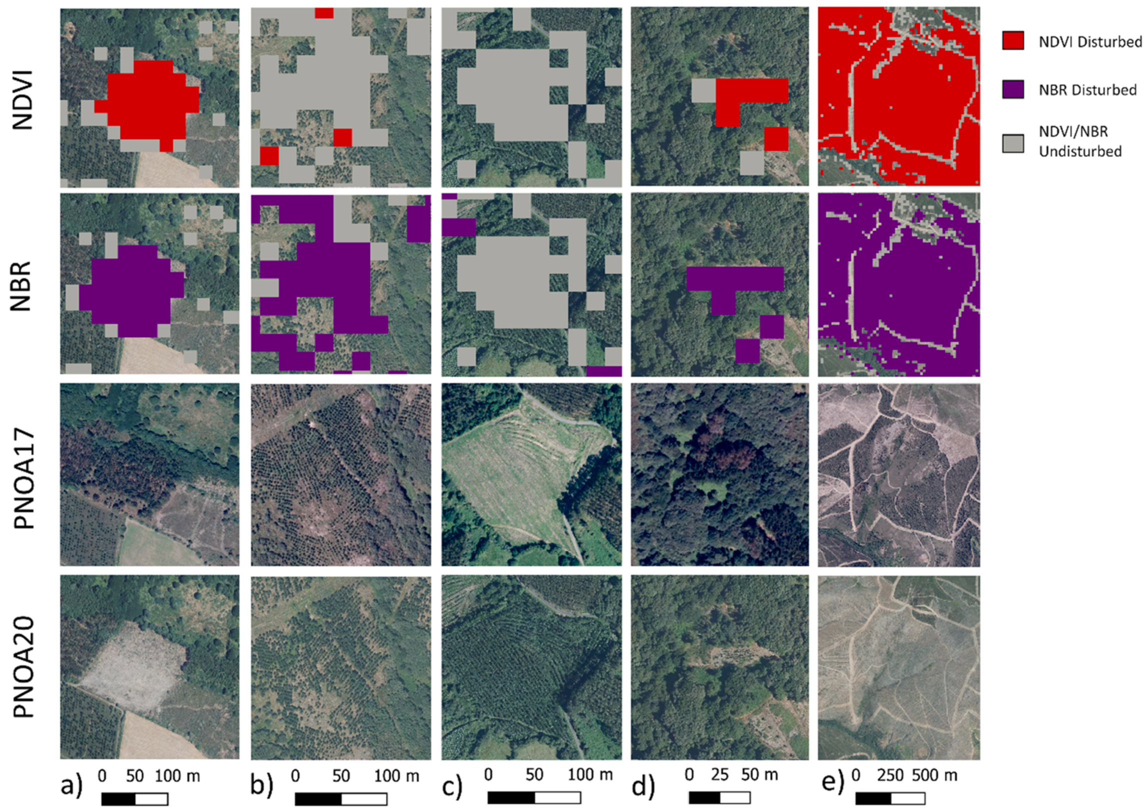

Fig. 13. Examples of the performance of the decision trees. Red: pixels detected as a disturbance by the NDVI. Purple: pixels detected as a disturbance by the NBR. Gray: pixels detected as undisturbed by the NBR or the NDVI. A) A harvesting event that was correctly detected by the NDVI and by the NBR. B) An example of an error of commission when only applying the NBR. C) An example of an area correctly identified as undisturbed by both the NBR and the NDVI. D) An example of a very small harvest area correctly detected by both the NDVI and the NBR. E) A wildfire in a shrub area correctly detected by the NDVI and the NBR. (For interpretation of the references to color in this figure legend, the reader is referred to the web version of this article.)

Another advantage of this methodology is that, as it is not dependent upon long time series of data, it is compatible with new satellites with enhanced characteristics. For example, many recent land cover and forest mapping studies are incorporating images from PlanetScope (Lefulebe et al., 2022; Pickering et al., 2021; Rösch et al., 2022), a satellite with a very low revisit time (daily) and which provides images with a higher resolution (3 m) than the Sentinel-2 images. The increased spatial resolution of PlanetScope makes it an appealing alternative for mapping regions such as Galicia that require a high level of spatial detail.

5. Conclusion

The presented methodology has proven to be robust and efficient at detecting forest disturbances in a large area with varying land covers, topographic conditions, and phenologies, and even in areas with a high degree of stand fragmentation. The workflow can be integrated with the land cover mapping methodology developed for the Continuous Galician Forest Inventory. This method allows the detection of small forest disturbances and their inclusion in annual land cover maps. It does not require the acquisition of additional data nor long time series of satellite images, which is valuable as it reduces computational time and the amount of information that must be stored, without sacrificing spatial resolution. Additionally, this means that it could potentially be used with new, enhanced satellite imagery in the future.

Finally, although specifically designed for the case of Galicia, this methodology could be applied to any land cover map production workflow based on time-series satellite imagery. For many agencies that have already developed their own time-series land cover maps, this method could facilitate the integration of land cover change detection into their maps.

Funding

This project was funded by the Administration of Rural Areas of the Government of Galicia under Grant 2020CONVINVENTARIOFORESTALR002; by the Spanish Ministry of Sciences, Innovation and Universities under the grant FPU19/02054; and the Spanish Ministry of Sciences, Innovation and Universities under Grant PID2019-111581RB-I00; Spanish Ministry of Sciences, Innovation and Universities under grant PID2019- 111581RB-I00 project PALEOINTERFACE: STRATEGIC ELEMENT FOR THE PREVENTION OF FOREST FIRES, DEVELOPMENT OF MULTISPECTRAL AND 3D ANALYSIS METHODOLOGIES FOR INTEGRATED MANAGEMENT.

CRediT authorship contribution statement

Alonso L.: Conceptualization, Data curation, Formal analysis, Investigation, Methodology, Funding acquisition, Software, Supervision, Validation, Visualization, Writing – original draft, Writing – review & editing. **Picos J.:** Conceptualization, Funding acquisition, Project administration, Resources, Supervision, Validation. **Armesto J.:** Conceptualization, Funding acquisition, Project administration, Resources, Validation.

Declaration of Competing Interest

The authors declare that they have no known competing financial interests or personal relationships that could have appeared to influence the work reported in this paper.

Data availability

The authors do not have permission to share data.

References

Abercrombie, S., Friedl, M., 2015. Improving the consistency of multitemporal land cover maps using a Hidden Markov Model. IEEE Trans. Geosci. Remote Sens. 54, 1–11. https://doi.org/10.1109/TGRS.2015.2463689.

Addo-Fordjour, P., Ankomah, F., 2017. Patterns and drivers of forest land cover changes in tropical semi-deciduous forests in Ghana. J. Land Use Sci. 12 (1), 71–86. https://doi.org/10.1080/1747423X.2016.1241313.

Alonso, L., Picos, J., Armesto, J., 2021. Forest land cover mapping at a regional scale using multi-temporal Sentinel-2 Imagery and RF Models. Remote Sens. 13, 2237. https://doi.org/10.3390/rs13122237.

Alonso, L., Picos, J., Armesto, J., 2022a. Automatic identification of forest disturbance drivers based on their geometric pattern in Atlantic Forests. Remote Sens. 14, 697. https://doi.org/10.3390/rs14030697.

Alonso, L., Rodríguez, A., Picos, J., Armesto, J., 2022b. Challenges in automatic forest changes through land cover mapping. Int. J. For. Res., Pending Publication. https://doi.org/10.1093/forestry/cpac053.

Breiman, L., Friedman, J.H., Olshen, R.A., Stone, C.J., 1984. *Classification and Regression Trees*; Wadsworth: Boca Raton. FL, USA.

Buchhorn, M., Bertels, L., Smets, B., De Roo, B., Lesiv, M., Tsendbazar, N.E., Masiliunas, D., Li, L., 2021. Copernicus Global Land Service: Land Cover 100m: version 3 Globe 2015-2019: Algorithm Theoretical Basis Document (Dataset v3.0, doc issue 3.4). Zenodo. https://doi.org/10.5281/zenodo.4723924.

Buchhorn, M., Lesiv, M., Tsendbazar, N.-E., Herold, M., Bertels, L., Smets, B., 2020. Copernicus global land cover layers—collection 2. Remote Sens. 12, 1044. https://doi.org/10.3390/rs12061044.

Bueno, I.T., McDermid, G.J., Silveira, E.M.O., Hird, J.N., Domingos, B.I, Acerbi Júnior, F. W., 2020. Spatial agreement among vegetation disturbance maps in tropical domains using Landsat time series. Remote Sens., 12, 2948. https://doi.org/10.3390/rs12182948.

Cardille, J.A., Perez, E., Crowley, M.A., Wulder, M.A., White, J.C., Hermosilla, T., 2022. Multi-sensor change detection for within-year capture and labelling of forest disturbance. Remote Sens. Environ. 268, 112741. https://doi.org/10.1016/j.rse.2021.112741.

Chen, N., Tsendbazar, N.E., Hamunyela, E., Verbesselt, J., Herold, M., 2021b. Sub-annual tropical forest disturbance monitoring using harmonized Landsat and Sentinel-2 data. Int. J. Appl. Earth Observ. Geoinform. 102, 102386. https://doi.org/10.1016/j.jag.2021.102386.

Chen, S., Woodcock, C.E., Bullock, E.L., Arévalo, P., Torchinava, P., Peng, S., Olofsson, P., 2021a. Monitoring temperate forest degradation on Google Earth Engine using Landsat time series analysis. Remote Sens. Environ. 265, 112648. https://doi.org/10.1016/j.rse.2021.112648.

Congalton, R.G., Gu, J., Yadav, K., Thenkabail, P., Ozdogan, M., 2014. Global land cover mapping: a review and uncertainty analysis. Remote Sens. 6, 12070–12093. https://doi.org/10.3390/rs61212070.

Copernicus, 2020, Copernicus Global Land Service. https://land.copernicus.eu/global/products/lc (accessed 9 December 2022).

Corbelle-Rico, E., Sánchez-Fernández, P., López-Iglesias, E., Lago-Peñas, S., Da-Rocha, J. M., 2022. Putting land to work: An evaluation of the economic effects of recultivating abandoned farmland. Land Use Policy 112, 105808. https://doi.org/10.1016/j.landusepol.2021.105808.

Xunta de Galicia, 2016. 1ª revisión del plan forestal de galicia. Documento diagnóstico del monte y el sector forestal gallego. https://mediorural.xunta.gal/sites/default/files/temas/forestal/plan-forestal/1_revision_plan_forestal_cast.pdf (accessed 9 December 2022).

Xunta de Galicia, 2022b. Sistema de indicadores da administración dixital. Producción forestal. https://indicadores-forestal.xunta.gal/portal-bi-internet/dashboard/Dashboard.action?selectedScope=OBSFOR_BI_A02_INT&selectedLevel=OBSFOR_BI_2_INT.L0&selectedUnit=12&selectedTemporalScope=2&selectedTemporal=31/12/2020 (accessed on 09 December 2021).

EEA (European Environment Agency), 2021, Copernicus Land Monitoring Service – Corine Land Cover. https://www.eea.europa.eu/data-and-maps/data/copernicus-land-monitoring-service-corine (accessed 12 December 2022).

ESA (European Space Agency) and SEOM (Scientific Exploitation of Operational Missions), 2017. S2GLC, Sentinel-2 Global Land Cover. https://s2glc.cbk.waw.pl/ (accessed 12 December 2022).

ESA (European Space Agency), 2015. Sentinel-2. https://www.esa.int/Space_in_Member_States/Spain/SENTINEL_2 (accessed 9 December 2022).

Esteban Cava, J., Tomé, J.L., García Castillo, D., Salvador, M., Pérez Oleaga, A. 2022. Aplicación de la teledetección a la certificación forestal en Galicia. *8°Congreso forestal Español. Sociedad Española de Ciencias Forestales.* ISBN 978-84-941695-6-4. https://8cfe.congresoforestal.es/sites/default/files/actas/8CFE-742.pdf.

European Commission, ESA, Copernicus, 2022. Copernicus Open Access Hub. (accessed 9 December 2022).

FAO, 2020. Global forest resources assessment 2020. Terms and Definitions. Forest Resources Assessment Working Paper 188, Rome.

Gao, Y., Quevedo, A., Szantoi, Z., Skutsch, M., 2019. Monitoring forest disturbance using time-series MODIS NDVI in Michoacán, Mexico. Geocarto Int. 36 (15), 1768–1784. https://doi.org/10.1080/10106049.2019.1661032.

Gao, Y., Solórzano, J.V., Quevedo, A., Loya-Carrillo, J.O., 2021. How BFAST trend and seasonal model components affect disturbance detection in tropical dry forest and temperate Forest. Remote Sens. 13, 2033. https://doi.org/10.3390/rs13112033.

Giannetti, F., Pegna, R., Francini, S., McRoberts, R.E., Travaglini, D., Marchetti, M., Scarascia Mugnozza, G., Chirici, G., 2020. A new method for automated clearcut disturbance Detection in Mediterranean coppice forests using Landsat time series. Remote Sens. 12, 3720. https://doi.org/10.3390/rs12223720.

Gilani, H., Naz, H., Arshad, M., Nazim, K., Akram, U., Abrar, A., Asif, M., 2020. Evaluating mangrove conservation and sustainability through spatiotemporal (1990–2020) mangrove cover change analysis in Pakistan. Estuar. Coast. Shelf Sci. 249 https://doi.org/10.1016/j.ecss.2020.107128.

Gorelick, N., Hancher, M., Dixon, M., Ilyushchenko, S., Thau, D., Moore, R., 2017. Google Earth Engine: Planetary-scale geospatial analysis for everyone. Remote Sens. Environ. 202, 18–27. https://doi.org/10.1016/j.rse.2017.06.031.

Gyamfi-Ampadu, E., Gebreslasie, M., 2021. Two decades progress on the application of remote sensing for monitoring tropical and sub-tropical natural forests: a review. Forests 12, 739. https://doi.org/10.3390/f12060739.

Hamunyela, E., Rosca, S., Mirt, A., Engle, E., Herold, M., Gieseke, F., Verbesselt, J., 2020. Implementation of BFAST monitor Algorithm on Google Earth Engine to support large-area and sub-annual change monitoring using Earth observation data. Remote Sens. (Basel) 12 (18), 2953. https://doi.org/10.3390/rs12182953.

Hislop, S., Jones, S., Soto-Berelov, M., Skidmore, A., Haywood, A., Nguyen, T.H., 2019. A fusion approach to forest disturbance mapping using time series ensemble techniques. Remote Sens. Environ. 221, 188–197. https://doi.org/10.1016/j.rse.2018.11.025.

Inglada, J., Vincent, A., Arias, M., Tardy, B., Morin, D., Rodes, I., 2017. Operational high resolution land cover map production at the country scale using satellite image time series. Remote Sens. 9, 95. https://doi.org/10.3390/rs9010095.

JCyL (Junta de Castilla y León), 2022. Mapa de cultivos y superficies naturales. http://mcsncyl.itacyl.es/ (accessed 12 December 2022).

Kennedy, R.E., Yang, Z., Cohen, W.B., 2010. Detecting trends in forest disturbance and recovery using yearly Landsat time series: 1. LandTrendr—Temporal segmentation algorithms. Remote Sens. Environ. 114, 2897–2910. https://doi.org/10.1016/j.rse.2010.07.008.

Key, C.H., Benson, N.C., 2003. The normalized burn ratio (NBR): A Landsat TM radiometric measure of burn severity. US Geological Survey Northern Rocky Mountain Science Center. U.S. Department of the Interior, U.S. Geological Survey, Northern Rocky Mountain Science Center.

Kogan, F.N., 1995. Droughts of the late 1980s in the United States as derived from NOAA polar-orbiting satellite data. Bull. Am. Meteorol. Soc. 76 (5), 655–668. https://doi.org/10.1175/1520-0477(1995)076<0655:DOTLIT>2.0.CO;2.

Kukawska, E., Lewiński, S., Krupiński, M., Malinowski, R., Nowakowski, A., Rybicki, M., Kotarba, A., 2017. Multitemporal Sentinel-2 Data—Remarks and Observations. In: In Proceedings of the 2017 9th International Workshop on the Analysis of Multitemporal Remote Sensing Images (MultiTemp), pp. 2–5.

Lefulebe, B.E., Van der Walt, A., Xulu, S., 2022. Fine-scale classification of urban land use and land cover with planetscope imagery and machine learning strategies in the City of Cape Town, South Africa. Sustainability 14, 9139. https://doi.org/10.3390/su14159139.

Levers, C., Verkerk, H., Müller, D., Verburg, P., Butsic, V., Leitão, P., Lindner, M., Kuemmerle, T., 2014. Drivers of forest harvesting intensity patterns in Europe. For. Ecol. Manage. 315, 160–172. https://doi.org/10.1016/j.foreco.2013.12.030.

López-Amoedo, A., Álvarez, X., Lorenzo, H., Rodríguez, J.L., 2021. Multi-Temporal Sentinel-2 data analysis for smallholding forest cut control. Remote Sens. 13, 2983. https://doi.org/10.3390/rs13152983.

Lv, Z., Liu, T., Zhang, P., Atli Benediktsson, J., Chen, Y., 2018. Land cover change detection based on adaptive contextual information using bi-temporal remote sensing images. Remote Sens. 10, 901. https://doi.org/10.3390/rs10060901.

Malinowski, R., Lewiński, S., Rybicki, M., Gromny, E., Jenerowicz, M., Krupiński, M., Nowakowski, A., Wojtkowski, C., Krupiński, M., Krätzschmar, E., Schauer, P., 2020. Automated production of a land cover/use map of Europe Based on Sentinel-2 Imagery. Remote Sens. 12, 3523. https://doi.org/10.3390/rs12213523.

Mandal, M.S.H., Hosaka, T., 2020. Assessing cyclone disturbances (1988–2016) in the Sundarbans mangrove forests using Landsat and Google Earth Engine. Nat Hazards 102, 133–150. https://doi.org/10.1007/s11069-020-03914-z.

MAPA, 2019. Los Incendios Forestales en España. Decenio 2006 – 2015, MAPA, Madrid 2019. https://www.miteco.gob.es/es/biodiversidad/temas/incendios-forestales/incendios-decenio-2006-2015_tcm30-521617.pdf (accessed 9 December 2022).

MAPA, 2021. Estadísticas de incendios forestales. Available online: https://www.miteco.gob.es/es/biodiversidad/estadisticas/Incendios_default.aspx (accessed on 9 December 2022).

Masiliūnas, D., Tsendbazar, N.-E., Herold, M., Verbesselt, J., 2021. BFAST Lite: a lightweight break detection method for time series analysis. Remote Sens. 13, 3308. https://doi.org/10.3390/rs13163308.

Meteogalicia,, 2022. Meteogalicia. accessed 9 December 2022. https://www.meteogalicia.gal/web/inicio.action.

Mi, J., Liu, L., Zhang, X., Chen, X., Yuan, G., Xie, S., 2022. Impact of geometric misregistration in GlobeLand30 on land-cover change analysis, a case study in China. J. Appl. Remote Sens. 16 (1), 014516. https://doi.org/10.1117/1.JRS.16.014516.

MITERD (Ministerio para la Transición Ecológica y el Reto Demográfico), 2018. Anuario de estadística forestal. https://www.mapa.gob.es/es/desarrollorural/estadisticas/aef_2018_documentocompleto_tcm30- 543070.pdf (accessed 9 December 2022).

MLRLC (Multi-Resolution Land Characteristics Consortium), 2019. National Land Cover Database (NLCD) 2019. accessed 12 December 2022. https://www.mrlc.gov/.

MTMAU (Ministerio de Transporte Movilidad y Agenda Urbana) and IGN (Instituto geográfico Nacional), 2022. Centro de Descargas. Centro Nacional de Información Geográfica. http://centrodedescargas.cnig.es/CentroDescargas/index.jsp (accessed 9 December 2022).

MTMAU (Ministerio de Transporte Movilidad y Agenda Urbana), 2022. Plan Nacional de Ortofotografía Aérea (PNOA). https://pnoa.ign.es/ (accessed 9 December 2022).

Nitoslawski, S. A., Wong-Stevens, K., Steenberg, J. W. N., Witherspoon, K., Nesbitt, L., Konijnendijk van den Bosch, C. C., 2021. The digital forest: Mapping a decade of knowledge on technological applications for forest ecosystems. *Earth's Future*, 9, e2021EF002123. https://doi.org/10.1029/2021EF002123.

Pickering, J., Tyukavina, A., Khan, A., Potapov, P., Adusei, B., Hansen, M.C., Lima, A., 2021. Using multi-resolution satellite data to quantify land dynamics: applications of PlanetScope imagery for cropland and tree-cover loss area estimation. Remote Sens. 13, 2191. https://doi.org/10.3390/rs13112191.

QGIS.org, 2022. QGIS Geographic Information System. QGIS Association. http://www.qgis.org (accessed 9 December 2022).

R Core Team, 2020. R: A language and environment for statistical computing. R Foundation for Statistical Computing, Vienna, Austria https://www.R-project.org/ (accessed 16 March 2023.

Rösch, M., Sonnenschein, R., Buchelt, S., Ullmann, T., 2022. Comparing PlanetScope and Sentinel-2 imagery for mapping mountain pines in the Sarntal Alps. Italy. *Remote Sens.* 14, 3190. https://doi.org/10.3390/rs14133190.

Serviglobal,, 2022. Regional Land Cover Monitoring System – Hindu Kush Himalaya. accessed 12 December 2022. https://www.servirglobal.net/ServiceCatalogue/details/5bc986a651ebdcae79683361.

Shen, J., Chen, G., Hua, J., Huang, S., Ma, J., 2022. Contrasting forest loss and gain patterns in subtropical china detected using an integrated LandTrendr and machine-learning method. Remote Sens. 14, 3238. https://doi.org/10.3390/rs14133238.

Spanish government, 2011. Ministerio de Hacienda. Sede Electrónica del Catastro. https://www.sedecatastro.gob.es (accessed 9 December 2022).

Tarpley, J.D., Schneider, S.R., Money, R.L., 1984. Global vegetation indices from the NOAA-7 meteorological satellite. J. Clim. Appl. Meteorol. 23, 491–494. https://doi.org/10.1175/1520-0450(1984)023<0491:GVIFTN>2.0.CO;2.

Therneau, T.; Atkinson, B. Rpart: Recursive Partitioning and Regression Trees. R Package Version 4.1-15. 2019. Available online: https://CRAN.R-project.org/package=rpart (accessed on 9 December 2021).

Tian, L., Wang, J., Zhou, H., Wang, J., 2018. Automatic detection of forest fire disturbance based on dynamic modelling from MODIS time-series observations. Int. J. Remote Sens. 39 (12), 3801–3815. https://doi.org/10.1080/01431161.2018.1437294.

UKCEH (UK Environmental Information Data Centre),, 2021. The UKCEH Land Cover Map for 2020. accessed 12 December 2022. https://www.ceh.ac.uk/sites/default/files/2021-11/lcm2020ProductDocumentation.pdf.

Verbesselt, J., Hyndman, R., Newnham, G., Culvenor, D., 2010. Detecting trend and seasonal changes in satellite image time series. Remote Sens. Environ. 114 (1), 106–115. https://doi.org/10.1016/j.rse.2009.08.014.

Verbesselt, J., Zeileis, A., Herold, M., 2012. Near real-time disturbance detection using satellite image time series. Remote Sens. Environ. 123, 98–108. https://doi.org/10.1016/j.rse.2012.02.022.

Vieilledent, G., Grinand, C., Rakotomalala, F.A., Ranaivosoa, R., Rakotoarijaona, J.R., Allnutt, T.F., Achard, F., 2018. Combining global tree cover loss data with historical national forest cover maps to look at six decades of deforestation and forest fragmentation in Madagascar. Biol. Conserv. 222, 189–197. https://doi.org/10.1016/j.biocon.2018.04.008.

Wulder, M.A., Coops, N.C., Roy, D.P., White, J.C., Hermosilla, T., 2018. Land Cover 2.0. Int. J. Remote Sens. 39, 4254–4284. https://doi.org/10.1080/01431161.2018.1452075.

Xu, L., Herold, M., Tsendbazar, N.E., Masiliūnas, D., Li, L., Lesiv, M., Fritz, S., Verbesselt, J., 2022. Time series analysis for global land cover change monitoring: A comparison across sensors. Remote Sens. Environ. 271, 112905. https://doi.org/10.1016/j.rse.2022.112905.

Xunta de Galicia, 2022. Inventario forestal Continuo de Galicia. accessed 9 December 2022. https://invega.xunta.gal/invega/web/.

Zhou, G., Liu, M., Liu, X., 2021. An autoencoder-based model for forest disturbance detection using Landsat time series data. Int. J. Digital Earth 14 (9), 1087–1102. https://doi.org/10.1080/17538947.2021.1949399.

Zhu, L., Shi, R., Peng, S., 2020. Removing land cover spurious change by geo-eco zoning rule base. *ISPRS - International Archives of the Photogrammetry, Remote Sensing and Spatial.* Inf. Sci. XLII-3/W10, 677–683. https://doi.org/10.5194/isprs-archives-XLII-3-W10-677-2020.

Zhu, Z., Woodcock, C.E., 2014. Continuous change detection and classification of land cover using all available Landsat data. Remote Sens. Environ. 144, 152–171. https://doi.org/10.1016/j.rse.2014.01.011.